Eur. Phys. J. A (2023) 59:16
https://doi.org/10.1140/epja/s10050-023-00931-x

THE EUROPEAN PHYSICAL JOURNAL A

Regular Article -Theoretical Physics

Nuclear properties for nuclear astrophysics studies

S. Goriely[a]

Institut d'Astronomie et d'Astrophysique, CP-226, Université Libre de Bruxelles, 1050 Brussels, Belgium

Received: 3 November 2022 / Accepted: 23 January 2023
© The Author(s), under exclusive licence to Società Italiana di Fisica and Springer-Verlag GmbH Germany, part of Springer Nature 2023
Communicated by N. Alamanos

Abstract The need for nuclear data for astrophysics applications challenges experimental techniques as well as the robustness and predictive power of present nuclear models. Most of the nuclear data evaluations and predictions are still performed on the basis of phenomenological nuclear models. In the last decades, important progress has been achieved in fundamental nuclear physics, making it now feasible to use more reliable, but also more complex microscopic or semi-microscopic models in the evaluation and prediction of nuclear data for practical applications. In the present contribution, the reliability and accuracy of recent nuclear theories are discussed for most of the quantities needed to estimate reaction cross sections and beta-decay rates, namely nuclear masses, nuclear level densities, gamma-ray strength, fission properties and beta-strength functions. It is shown that nowadays, mean-field models can be tuned at the same level of accuracy as the phenomenological models, renormalized on experimental data if needed, and therefore can replace the phenomenological inputs in the prediction of nuclear data. While fundamental nuclear physicists keep on improving state-of-the-art models, in particular the shell or ab-initio models, nuclear applications could make use of their most recent results as quantitative constraints or guides to improve the predictions in energy or mass domain that will remain inaccessible experimentally.

1 Introduction

Among the various fields in nuclear astrophysics, stellar evolution and nucleosynthesis are clearly the most closely related to nuclear physics. The imprint of nuclear physics can be found in the origin of almost all nuclides produced in the Universe and is a fundamental ingredient to estimate the energy generation in stars [1,2]. Impressive progress has been made for the last decades in the different fields related to nucleosynthesis and stellar evolution, especially in experimental and theoretical nuclear physics, as well as in ground-based or space astronomical observations and astrophysical modellings. In spite of that success, major problems and puzzles remain. In particular, experimental nuclear data only covers a minute fraction of the whole set of data required for nucleosynthesis applications. Reactions of interest often concern unstable or even exotic (neutron-rich, neutron-deficient, superheavy) species for which no experimental data exist. In addition, a large number (thousands) of unstable nuclei may be involved for which many different properties have to be determined (Fig. 1). The energy range for which measurements are available is also restricted to the small range reachable by present experimental setups. An additional serious difficulty comes from the fact that the nuclei are immersed in a stellar environments which may have a significant impact on their static properties, the diversity of their transmutation modes, some of which are not observable in the laboratory, and on the probabilities of these modes. The description of nuclei as individual entities has even to be replaced by the construction of an equation of state at the high temperatures and/or densities prevailing in the cores of exploding stars and in compact objects (neutron stars). To fill the gaps, theoretical predictions are the only choice.

Nuclear reactions and decays represent the fundamental ingredients of all nucleosynthesis models. Two major classes of nuclear reactions are invoked, the thermonuclear reactions and the non-thermal transformations also known as spallation reactions. Thermonuclear reactions took place at the primordial or cosmological (Big-Bang) level as well as inside the stars throughout galactic evolution. On the other hand, spallation reactions are important in diluted and cold medium, as the interstellar medium, through the interaction with galactic cosmic rays (GCR), and at the surface of stars or in their surroundings through interaction with energetic stellar particles [4].

[a] e-mail: sgoriely@astro.ulb.ac.be (corresponding author)

Published online: 06 February 2023

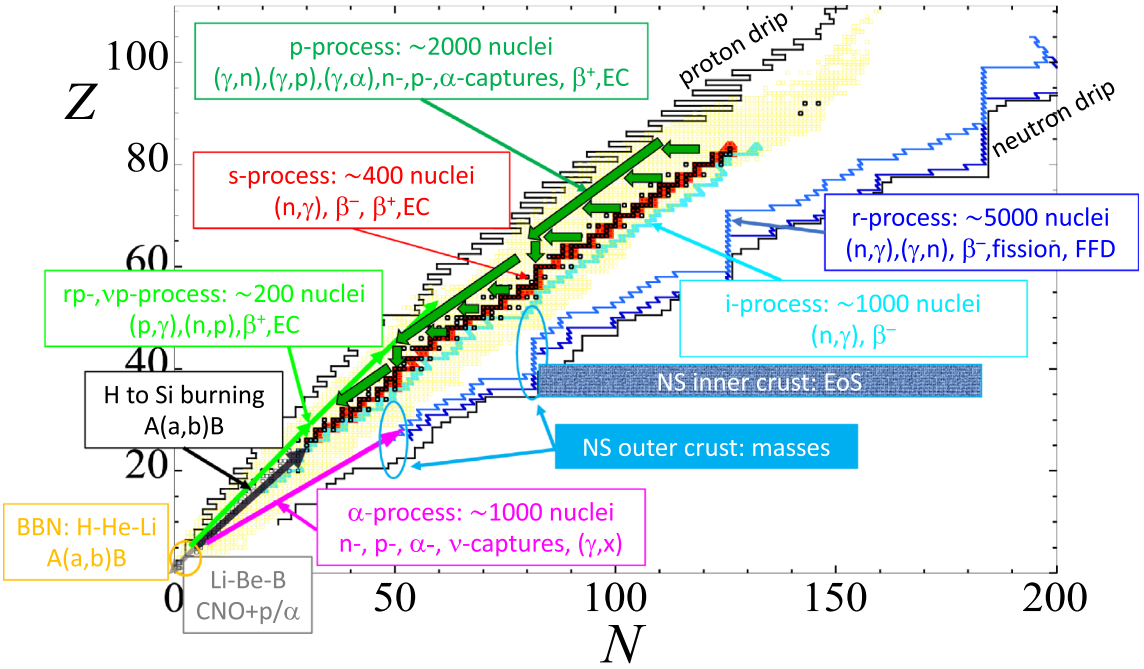

Fig. 1 Schematic representation in the (N, Z) plane of the different nuclear astrophysics applications, including nucleosynthesis processes, composition and structure properties of neutron stars (NS). For each process, the nuclear needs are listed. The open black squares correspond to stable or long-lived nuclei, the yellow squares to the nuclei for which masses have been measured and are included in the 2020 atomic mass evaluation (AME) [3]. Nuclei with neutron or proton separation energies tending to zero define the neutron or proton "drip lines" (solid black lines), as predicted from a mass model. More details can be found in Ref. [1] and in Sect. 2

The primordial Big-Bang nucleosynthesis (BBN) is responsible for the bulk He content of the Universe as well as for the synthesis of some other light nuclei, like D, ^{3}He and ^{7}Li [5]. All the other nuclides, as well as a fraction of the Galactic ^{7}Li, and maybe ^{3}He, result from thermonuclear reactions taking place inside the stars. The only exceptions concern the ^{6}Li, Be and B nuclei for which spallation reactions from the nuclear interaction of GCR (accelerated CNO nuclei) with the interstellar medium (mainly protons and α-particles) are invoked [4]. In stars, the thermonuclear reactions can be induced by charged particles (proton or α-particles) or neutrons. In the former case, the reactions mainly take place on light or medium heavy nuclei $A \lesssim 60$–70, since the reactions involving heavier species are not probable enough (because of the excessive Coulomb barrier) to play a significant role in stellar environments. The importance of the charged-particle-induced reactions is twofold, first they are fundamental for the energy production enabling the star to counterbalance its energy loss (energetic equilibrium) and second they locally modify the stellar content where they take place. The neutron-induced reactions are obviously not restricted to species lighter than Fe, since no Coulomb barrier exists in this case. However, these reactions do not contribute to the nuclear energy production, though they may, in specific scenarios, contribute to temperature evolution, the light curve and mass ejection, as for example in the case of NS mergers [6,7].

The origin of most of the elements lighter than those of the Fe group have been explained, mainly thanks to the direct link between their nucleosynthesis and the energetic evolution of stars [2,8,9]. However, the synthesis of nuclei heavier than Fe is far from being well understood at the present time. The major mechanisms called for to explain the production of the heavy nuclei are the slow neutron-capture process (or s-process) [10–14], occurring during the hydrostatic stellar burning phases, the intermediate neutron-capture process (or i-process) taking place mainly in low-metallicity asymptotic giant branch (AGB) stars or rapidly accreting white dwarfs [15–21], the rapid neutron-capture process (or r-process) believed to develop during NS mergers or potentially, the explosion of a star as a supernova [1,22,23], and the p-process occurring in core-collapse supernova (CCSN) or Type-Ia supernovae (SNIa) [24–26]. These nucleosynthesis processes are shortly summarized in Sect. 2.

Strong, weak and electromagnetic interaction processes play an essential role in nuclear astrophysics. As shown in Fig. 1, a very large amount of nuclear information is necessary in order to model the various nucleosynthesis and stellar evolution processes. These concern the decay properties of a large variety of light to heavy nuclei between the

proton and neutron drip lines, including the β-decay or electron capture rates as well as α-decay or spontaneous fission probabilities for the heavy species. For the nuclei lighter than iron, most of the reactions involved during the BBN or the H- to Si-burning stages concern the capture of protons and α-particles at relatively low energies (far below 1 MeV for neutrons and the Coulomb barrier for charged particles). A limited number of fusion reactions involving heavy ions (^{12}C, ^{16}O) are also of direct impact during C and O-burning phases. These charged-particle induced reactions are described in Sect. 3.1. The nuclear data needed to explain the Li–Be–B nucleosynthesis is quite different since it mainly involves spallation reactions between CNO nuclei accelerated at high energies interacting with the interstellar H and He. A review of the relevant reactions and the precision at which they are needed can be found in Ref. [27]. When dealing with neutron capture s-, i- and r-processes of nucleosynthesis, experimental cross sections are only available for stable nuclei, so that resort to theory is needed in many cases. These are detailed in Sect. 3.2. When not available experimentally, reaction or decay rates need to be estimated theoretically and to do so additional nuclear properties, such as ground state structure properties, nuclear level densities (NLD), optical potentials, γ-ray strength functions, fission properties or β-strength functions, need to be derived, as discussed in Sect. 4. Since β-decays play a fundamental role for nucleosynthesis applications, models available for large-scale calculations and application to the r-process nucleosynthesis, in particular, are rapidly described in Sect. 5. Finally, conclusions are drawn in Sect. 6.

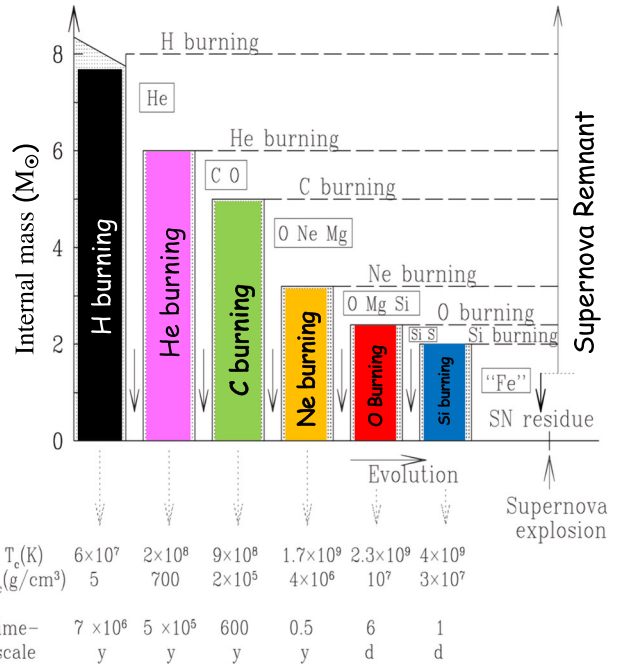

Fig. 2 Highly schematic representation in a classical one-dimensional approximation of the evolution of the internal structure of a spherically-symmetric massive star with M $\approx$ 25 M$_\odot$ (M$_\odot$ is the mass of the Sun) with initial composition similar to the solar one.The shaded zones correspond to nuclear burning stages. A given burning phase starts in the central regions (the central temperatures T_c and densities ρ_c are indicated at the bottom of the figure), and then migrates into thin peripheral burning shells. In between the central nuclear burning phases are episodes of gravitational contraction (downward arrows). The chemical symbols represent the most abundant nuclear species left after each nuclear-burning mode ("Fe" symbolizes the iron-peak nuclei with $50 \lesssim A \lesssim 60$). In the depicted illustration, the star eventually explodes as a supernova. The most central parts may leave a "residue," while the rest of the stellar material is ejected into the interstellar medium, where it is observed as a supernova "remnant"

2 Stellar evolution and nucleosynthesis

2.1 Stellar burning stages

As pictured very schematically in Fig. 2, the evolution of the central regions of stars follows successive "controlled" thermonuclear burning stages where mechanical and energy equilibrium are established, and of phases of slow quasi-equilibrium gravitational contraction. The latter phases trigger a temperature increase, while the former ones produce nuclear energy through charged-particle induced reactions leading at the same time to a change of the core composition. The sequence of nuclear burning episodes develops in time with nuclear fuels of increasing charge number Z and at temperatures increasing from several tens of 10^6 K to about 4×10^9 K [2,8,9,28,29]. Concomitantly, the duration of the successive nuclear-burning phases decreases in a dramatic way. This situation results from the combination of a decreasing energy production when going from H burning to the later burning stages and an increasing neutrino production, and the consequent energy losses, with temperatures in excess of about 5×10^8 K. The various hydrostatic and explosive nuclear burning modes from hydrogen to silicon burning and the corresponding energy production and nucleosynthesis are described in detail in Refs. [2,8,9,29].

2.2 The s-process

For the last decades, an extremely intense amount of work has been devoted to the slow neutron-capture process (or s-process) of nucleosynthesis called for to explain the origin of the stable nuclides heavier than iron located at the bottom of the valley of nuclear stability [10–13].

Even though the observation of the radioactive Tc element in stellar envelopes clearly proves that the s-process takes place during hydrostatic burning phases of a star, it remains difficult to explain the origin of the large neutron concentrations required to produce s-elements. Two nuclear reactions are suggested as possible neutron sources, i.e. ^{13}C(α,n)^{16}O

and ^{22}Ne(α,n)^{25}Mg. These reactions could be responsible for a large production of neutrons during given burning phases, namely the core He-burning of massive stars (heavier than 10 $M_\odot$) and the shell He-burning during the thermal AGB instabilities – known as thermal pulses (TP) – of low and intermediate mass stars (lower than typically 10 $M_\odot$).

As reviewed in great detail in Ref. [12], the s-process in AGB stars is thought to occur in their He-burning shell surrounding a nuclearly inert C–O core, either during recurrent and short convective TP episodes or in between these pulses. A rather large diversity of s-nuclide abundance distributions are predicted. A fraction of the synthesized s-nuclides (along with other He-burning products) could then be dredged-up to the surface shortly after each TP. In low-mass AGB stars (less than typically 3 $M_\odot$), it is generally considered that the necessary neutrons for the development of the s-process are mainly provided by ^{13}C(α,n)^{16}O, which can operate at temperatures around (1–1.5) $\times 10^8$ K. The efficiency of this mechanism is predicted to be the highest in stars with metallicities lower than solar ([Fe/H] $\ll$ 0). The astrophysical models underlying the TP scenario are still quite uncertain, in particular in the description of the mechanisms that could be at the origin of the neutron production. The neutron production in these locations depends sensitively on the mechanism of proton ingestion into underlying He-rich layers in amounts and at temperatures that allows the operation of the ^{12}C(p,γ)^{13}N(β^+)^{13}C(α,n)^{16}O where the production of ^{14}N by ^{13}C(p,γ)^{14}N is inefficient enough to avoid the hold-up of neutrons by the ^{14}N neutron poison. TP-AGB models including empirical diffusive overshoot have been relatively successful to explain such a partial mixing of protons from the H-rich envelope into the C-rich layers during the third dredge-up [12,13,30], but it remains difficult to model consistently such mixing mechanisms in common one-dimensional models.

Massive stars, and more specifically their He-burning cores and, to some extent, their C-burning shells, are also predicted to be s-nuclide producers through the operation of the ^{22}Ne(α,n)^{25}Mg. This neutron source can indeed be active in these locations that are hotter than the He shell of AGB stars. In addition, ^{22}Ne burning can also be partially activated in the carbon burning shell of massive stars. Many calculations performed in the framework of realistic stellar models come to the classical conclusion that this site is responsible for a substantial production of the $70 \lesssim A \lesssim 90$ s-nuclides, and can in particular account for the solar system abundances of these species. It has also been shown that rotation can significantly affect the efficiency of the s-process, especially at low metallicity [14,31,32]. Because of the rotational mixing operating between the H-shell and He-core during the core helium burning phase, the abundant ^{12}C and ^{16}O isotopes in the convective He-burning core are mixed within the H-shell, boosting the CNO cycle and forming primary ^{14}N that finally leads to the synthesis of extra ^{22}Ne, hence an increased neutron production with respect to what is found in non-rotating massive stars. In this case, s-process nuclei beyond $A = 90$ up to the second s-process peak $A \simeq 138$ can be effectively produced.

2.3 The i-process

The s- and r-processes introduced very early in the development of the theory of nucleosynthesis have to be considered as the end members of a whole class of neutron capture mechanisms. Supported by some observations that were difficult to reconcile solely with a combination of the s- and r-processes, a process referred to nowadays as the intermediate process (or i-process) has been put forth, with neutron concentrations in the approximate 10^{13} to 10^{16} neutrons/cm^3 range. The mechanism envisaged to be responsible for this production is the ingestion of protons in He- and C-rich layers, leading to the production of ^{13}C through ^{12}C(p,γ)^{13}N(β^+)^{13}C followed by a substantial production of neutrons through ^{13}C(α,n)^{16}O. This is analogous to the mechanism already considered to be active in TP-AGB stars (Sect. 2.2), but the higher neutron concentrations are expected to result from the very low metallicity of the considered stars and the activation of ^{13}C(α,n)^{16}O in convective regions at higher temperatures (typically $\sim 2.5 \times 10^8$ K).

Various numerical scenarios have been proposed to host such conditions. These include the proton ingestion during core He flash in very low-metallicity low-mass stars, during the TP phase of massive AGB (super-AGB) stars of very low metallicity, during the post-AGB phase ("final TP"), during rapid accretion of H-rich material on white dwarfs, or during shell He burning in massive very low-metallicity Population II or III stars. While the contribution of the i-process to the global Galactic enrichment and more particularly to our solar system remains unclear, it is needed to explain the heavy element patterns observed in peculiar stars, several carbon enhanced metal-poor (CEMP) stars with simultaneous presence of s elements and Eu (so-called CEMP-r/s) stars, as well as the Sakurai's object V4334 Sgr. More information can be found in Refs. [16–20].

2.4 The r-process

The r-process of stellar nucleosynthesis is called for to explain the production of the stable (and some long-lived radioactive) neutron-rich nuclides heavier than iron that are observed in stars of various metallicities, as well as in the solar system. Reviews can be found in Refs. [1,22,23].

Nuclear-physics-based and astrophysics-free r-process models of different levels of sophistication have been constructed over the years [33]. They all have their merits and their shortcomings. The ultimate goal was to identify realistic sites for the development of the r-process. For long,

the CCSN of massive stars has been envisioned as the privileged r-process location. One- or multi-dimensional spherical or aspherical explosion simulations in connection with the r-process nucleosynthesis are reviewed in Refs. [1,22,23]. Progress in the modelling of CCSNe and γ-ray bursts has raised a lot of excitement about the so-called neutrino-driven wind environment [34]. However, until now a successful r-process cannot be obtained *ab initio* without tuning the relevant parameters of the neutrino-driven wind (neutron excess, entropy, expansion timescale) in a way that is not supported by the most sophisticated existing models [35,36]. Although these scenarios remain promising, especially in view of their potential to contribute to the Galactic enrichment significantly, they remain affected by large uncertainties associated mainly with the still incompletely understood mechanism responsible for the CCSN explosion and the persistent difficulties to obtain suitable r-process conditions in self-consistent dynamical explosion and NS cooling models [35,37]. In particular, a subclass of CCSNe, the so-called collapsars corresponding to the fate of rapidly rotating and highly magnetized massive stars and generally considered to be at the origin of observed long gamma-ray bursts, could be a potential r-process site [38–40]. The production of r nuclides in these events may be associated with jets predicted to accompany the explosion [41,42], or with the accretion disk forming around a newly born central black hole (BH) [43].

Since early 2000, special attention has been paid to NS mergers as r-process sites following the confirmation by hydrodynamic simulations that a non-negligible amount of matter could be ejected from the system. Newtonian [44], conformally flat general relativistic [45,46], as well as fully relativistic [47–51] hydrodynamical simulations of NS–NS and NS–BH mergers with microphysical equations of state have demonstrated that typically some $10^{-3}\,M_\odot$ up to more than $0.1\,M_\odot$ can become gravitationally unbound on roughly dynamical timescales due to shock acceleration and tidal stripping. Also the relic object (a hot, transiently stable hypermassive NS followed by a stable supermassive NS, or a BH-torus system), can lose mass through outflows driven by a variety of mechanisms [46].

Simulations of growing sophistication have confirmed that the ejecta from NS mergers are viable strong r-process sites up to the third abundance peak and the actinides. The r nuclide enrichment is predicted to originate from both the dynamical (prompt) material expelled during the NS-NS or NS-BH merger phase and from the outflows generated during the post-merger remnant evolution of the relic BH-torus system. The resulting abundance distributions are found to reproduce well the solar system distribution, as well as various elemental distributions observed in low-metallicity stars [23]. In addition, the ejected mass of r-process material, combined with the predicted astrophysical event rate (around $10\,\mathrm{My}^{-1}$ in the Milky Way) can account for the majority of r-material in our Galaxy. A fundamental observational piece of evidence that NS mergers are r-nuclide producers indeed comes from the very important 2017 gravitational-wave and electromagnetic kilonova detection of the GW170817 event [52–54].

Despite the recent success of nucleosynthesis studies for NS mergers, the details of r-processing in these events is still affected by a variety of uncertainties, both from the nuclear physics and astrophysics aspects. The r-process nucleosynthesis is also important for understanding the origin of the radionuclides that could be used to estimate an approximate age of the Galaxy, the so-called radio-cosmochronometers.

2.5 The p-process

The p-process of stellar nucleosynthesis is aimed at explaining the production of the stable neutron-deficient nuclides heavier than iron that are observed in the solar system, and up to now in no other galactic location (for a review see Ref. [25]). Various scenarios have been proposed to account for the bulk p-nuclide content of the solar system, as well as for deviations ("anomalies") with respect to the bulk p-isotope composition of some elements discovered in primitive meteorites. In contrast to the s-, i- and r-processes calling for neutron captures to explain the production of heavy elements, the p isotopes are produced by photodisintegration reactions on already-synthezised s and r nuclei. These photoreactions involve (γ,n), (γ,p), and (γ,α) reactions at stellar temperatures of the order of 2–3 $\times 10^9$ K.

The p nuclides are mostly produced in the final explosion of a massive star ($M \gtrsim 10\,M_\odot$) as a CCSN or in pre-explosive oxygen burning episodes [25]. The p-process can develop in the O–Ne layers of the massive stars explosively heated to peak temperatures ranging between 1.7 and 3.3×10^9 K [24,26]. The seeds for the p-process are provided by the s-process that develops before the explosion during core He-burning (see Sect. 2.2). In this way the O–Ne layers that experience the p-process are initially enriched in $70 \lesssim A \lesssim 90$ s-nuclides for solar metallicity stars. For rotating stars of sub-solar metallicity (typically around $Z = 10^{-3}$), the s-process yields up to the second peak $A \simeq 138$ can be significantly increased [14], enhancing at the same time the p-process yields during the CCSN explosion [55].

SNIa have also been suggested as a potential site for the p-process [56]. The p-process nucleosynthesis possibly accompanying the deflagration or delayed detonation regimes has been mainly studied in 1D simulations and shown to give rather similar overabundances as CCSN models [25,57]. However, the predicted SNIa p-nuclide yields suffer from large uncertainties affecting the adopted explosion models as well as the s-seed distributions, detailed information on the composition of the material that is pre-explosively transferred to the white dwarf being missing.

Despite the fact that p nuclei can be produced consistently with solar ratios over a wide range of nuclei in such scenarios, there remain deficiencies in a few regions, most particularly in the Mo–Ru region where the p isotopes are strongly underproduced. This fact motivates the search for alternative or additional ways to produce these nuclides. In particular, proton capture and photodisintegration processes in helium star cataclysmics have been suggested as a promising nucleosynthesis source [58]. Such an object is made of a carbon-oxygen white-dwarf with sub-Chandrasekhar mass ($M < 1.4M_{\odot}$) accumulating a He-rich layer at its surface. An alternative site proposed to explain the origin of the Mo and Ru p-nuclei is the p-rich neutrino driven wind in CCSNe where antineutrino absorptions in the proton-rich environment produce neutrons that are immediately captured by neutron-deficient nuclei [59].

3 Reaction rates of astrophysical interest

3.1 Charged-particle induced reactions

In a given astrophysical location, two factors dictate the variety of nuclear reactions that can act as energy producers and/or as nucleosynthetic agents. The abundances of the reactants have obviously to be high enough, and the lifetimes of the reactants against a given nuclear transmutation have to be short enough for this reaction to have time to operate during the evolutionary timescale of the astrophysical site under consideration.

The probability of a thermonuclear reaction in an astrophysical plasma is strongly dependent on some specific properties of this plasma. In this respect, two key guiding features are the distribution of the energies of the reacting partners, and the reaction cross section at a given energy. First, the reacting nuclei are, locally at least, in a state of thermodynamic equilibrium. In such conditions, all nuclear species obey a Maxwell–Boltzmann distribution of energies, from which it is easily inferred that the relative energies of the reaction partners also obey such a distribution. Second, the reaction cross section between charged nuclei is dominated by the probability of penetration of the Coulomb barrier of the interacting nuclei. As a result, the effective reaction rate is obtained by integrating the strongly energy-dependent reaction cross sections over the whole Maxwell–Boltzmann energy range. The resulting integrant exhibits a strong maximum, generally referred to as the Gamow peak (see e.g. Ref. [2]). It is centered on the "most effective energy" given by $E_0 = 0.1220(Z_1^2 Z_2^2 \mu)^{1/3} T_9^{2/3}$ MeV, where Z_1, Z_2 are the charge numbers and μ the reduced mass, and T_9 the temperature T expressed in 10^9 K. The Gamow peak is characterized by a width approximated by $\Delta = 4(E_0 k_B T/3)^{1/2}$, where k_B is the Boltzmann constant. The reactions thus mostly occur in the approximate window from $E_0 - n\Delta$ to $E_0 + n\Delta$ ($n = 2$–3), assuming the possible role of resonances is small. For this reason, the energy range of astrophysical relevance for reactions between charged particles is largely above the thermal energy $k_B T$ and much lower than the Coulomb barrier. For these reasons, the sequence of hydrostatic burning episodes is characterized by a limited number of reactions between nuclei with increasing charges, from H-burning to Si-burning, and the charged-particle induced thermonuclear reactions of relevance concern mainly the capture of protons or α-particles which offer the lowest Coulomb barriers. A limited number of fusion reactions involving heavy ions (^{12}C, ^{16}O) are also of great importance [2,8,9].

In non-explosive conditions, like in the quiescent phases of stellar evolution which take place at relatively low temperatures, most of the reactions of interest concern stable nuclides. Even so, the experimental determination of their charged-particle induced cross sections face enormous problems, and represent a real challenge [2]. This relates directly to the smallness of the cross sections due to the fact that E_0 lies well below the Coulomb barrier. As a consequence, the cross sections can dive into the nanobarn to picobarn range. Much experimental and theoretical effort has been devoted to the reactions involved in the H- and He-burning modes. They are available in various compilations [60–62].

In explosive situations, the temperatures are typically higher than in the non-explosive cases. The corresponding increase of the effective energies E_0 gives rise to a higher probability of penetration of the Coulomb barriers, and consequently larger cross sections. The price to pay to reach this higher energy domain is huge, however. The nuclear flows indeed depart strongly from the bottom of the valley of nuclear stability, and involve unstable nuclei, sometimes very close to the nucleon drip lines (see Fig. 1).

Finally, in stellar plasmas, a specific electron screening correction has to be applied, which can drastically affect the cross sections for bare nuclei [63,64]. This correction arises because of the ability of a nucleus to polarize its stellar surroundings. As a result, the Coulomb barrier seen by the reacting nuclei is modified in such a way that the tunneling probability, and consequently the reaction rate, increases over its value in vacuum conditions. Different formalisms have been developed depending on the ratio of the Coulomb energy of reacting nuclei to the thermal energy. Weak screening applies if this ratio is well below unity, while a strong screening is obtained when this ratio is well in excess of unity. In this case, a very large increase of the reaction rates is predicted. The limiting situation of strong screening is reached when solidification of the stellar plasma leads to the special pycnonuclear regime [63,64]. In this case, the reactions are not governed by temperature like in the thermonuclear regime, but instead by lattice vibrations in dense Coulomb solids. This limiting

regime can be approached, e.g. at the high densities and low temperatures prevailing in white dwarfs.

3.2 Neutron captures of astrophysical interest

The considerations above leading to the most effective energy in the case of reactions between charged particles do of course not apply to neutron captures in view of the absence of Coulomb barriers. In this case it can be shown that the most effective energy is of the order of $k_B T$, i.e. for the various s-, i- or r-processes in the range of 10–100 keV. Measurement of neutron capture cross sections (especially radiative neutron captures, as well as (n, p) and (n, α) reactions, and neutron-induced fission) at such energies of astrophysical interest have been under very active investigation over the last decades at a variety of facilities [2,65,66]. Various neutron production techniques as well as a diverse cross section measurement methods have been adopted. A successful feature is related to the property that neutrons produced by ^{7}Li(p,n)^{7}Be have an energy spectrum that closely resembles the thermalized Maxwellian stellar spectra in typical s-process conditions. The most suitable experimental procedures depend notably on the stability/instability of the targets and reaction products. Only the cross sections for the stable nuclides are known nowadays with a very good accuracy [67]. Experimental data are also available for some nuclides located close enough to the valley. The use of inverse reactions, particularly photodisintegrations, can help for constraining such data. At this point, one has to remember, however, that the experimental accuracy presently reached concerns the capture of neutrons by nuclei in their ground states, and is affected by the contribution to the reactions of target excited states, which can be evaluated by theory only. Some attempts to study the contribution of excited states have started with dedicated measurements of the super-elastic scattering cross sections on long-lived metastable states [68,69]. When not available experimentally, neutron capture rates need to be estimated theoretically, as discussed in Sect. 4.

4 Theoretical determination of reaction rates

As far as theory is concerned to complement missing experimental cross sections, most of the calculations for astrophysics applications are based on the statistical model of Hauser–Feshbach. Such a model makes the fundamental assumption that the capture process takes place with the intermediary formation of a compound nucleus (CN) in thermodynamic equilibrium. The energy of the incident particle is then shared more or less uniformly by all the nucleons before releasing the energy by particle emission or γ-de-excitation. The formation of a CN is usually justified by assuming that the level density in the compound nucleus at the projectile incident energy is large enough to ensure an average statistical continuum superposition of available resonances. The statistical model has proven its ability to predict cross sections accurately, within typically 50% for the particular case of radiative neutron captures. However, this model suffers from uncertainties stemming essentially from the predicted nuclear ingredients describing the nuclear structure properties of the ground and excited states, and the strong and electromagnetic interaction properties. Our capacity to predict reliably all these ingredients, i.e. the nuclear structure properties (masses, deformations, matter densities), the NLD, the optical potential, the γ-ray strength function, the fission properties, especially for exotic neutron-rich nuclei, are discussed below. The availability of experimental data as well as the various models developed are reviewed in Refs. [70–72].

When the number of available states in the CN is relatively small, the capture reaction is known to be possibly dominated by direct electromagnetic transitions to a bound final state rather than through a compound nucleus intermediary. This direct capture (DC) proceeds via the excitation of only a few degrees of freedom on much shorter time scale reflecting the time taken by the projectile to travel across the target. This mechanism can be satisfactorily described with the perturbative approach known as the potential model [73–77]. It is now well accepted that the DC is important, and often dominant at the very low energies of astrophysical interest for light or exotic nuclei systems for which few, or even no resonant states are available. The direct contribution to the neutron capture rate can be 2–3 orders of magnitude larger than the one obtained within the Hauser–Feshbach approach traditionally used in nucleosynthesis applications. Significant uncertainties still affect the DC predictions. These are related to the determination of the nuclear structure ingredients of relevance, i.e the nuclear mass, spectroscopic factor, neutron-nucleus interaction potential and excited level scheme. A special emphasis needs to be put on the determination of the low-energy excitation spectrum with all details of the spin and parity characteristics. This can be deduced from a NLD model, but not a statistical approach. An important effort needs to be made to improve the prediction of such nuclear inputs within reliable microscopic models. The transition from the CN to the DC mechanism when only a few resonant states are available also needs to be tackled in a more detailed way, for example within the Breit-Wigner approach [78].

For specific applications such as nuclear astrophysics, a large number of data needs to be extrapolated far away from the experimentally known region. In this case, two major features of the nuclear theory must be contemplated, namely its *reliability* and *accuracy*. A microscopic description by a physically sound model based on first principles ensures a reliable extrapolation away from experimentally known region. For this reason, use is made preferentially of

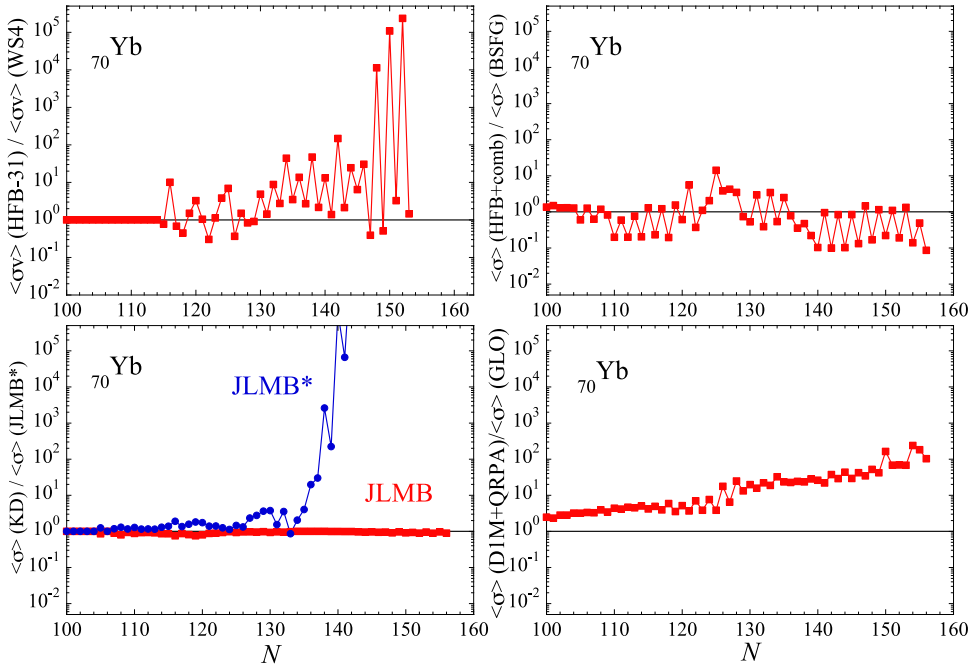

Fig. 3 Illustration of some uncertainties affecting the prediction of the radiative neutron capture rates (at $T = 10^9$K) calculated with the TALYS code [79] for the Yb isotopes ($Z = 70$), between the valley of β-stability and the neutron drip line; these include the sensitivity to the mass model (upper left), to the NLD (upper right), the optical potential (lower left) and γ-ray strength function (lower right). See text for more details

microscopic or semi-microscopic global predictions based on reliable nuclear models which, in turn, can compete with more phenomenological highly-parametrized models in the reproduction of experimental data. Global microscopic approaches have been developed for the last decades, tuned to provide estimates at the same level of accuracy as the phenomenological models, and renormalized on experimental data when needed. Such models can now replace the phenomenological inputs in astrophysical applications for which nuclear properties need to be predicted [80]. The impact of such microscopic or semi-microscopic global predictions with respect to more phenomenological approaches are illustrated in Fig. 3 for the neutron capture reaction rates along the Yb isotopic chains and seen to reach deviations of a few orders of magnitude when considering the most neutron-rich Yb isotopes. Such effects are further discussed below. Some of these theoretical models are described below for the various ingredients of interest in reaction rate calculations.

4.1 Nuclear masses

Among the ground state properties, the atomic mass is obviously the most fundamental quantity (for a review on atomic masses, see e.g. [81]). The calculation of the reaction cross section also requires the knowledge of other ground state properties, such as the deformation, density distribution or the single-particle level scheme. When not available experimentally, these quantities need to be extracted from a mass model which aims at reproducing measured masses as accurately as possible, i.e typically with a root-mean-square (rms) deviation of about 800 keV. The importance of estimating all ground state properties reliably should not be underestimated. For example, the NLD of a deformed nucleus at low energies (typically at the neutron separation energy) is predicted to be about 30–50 times larger than of a spherical one due principally to the rotational enhancement. An erroneous determination of the deformation can therefore lead to large errors in the estimate of radiative capture cross sections. For this reason, modern mass models not only try to reproduce at best experimental masses and mass differences, but also charge radii, quadrupole moments, giant resonances, fission barriers, shape isomers, infinite nuclear matter properties [81,82].

With a view to their astrophysical application in neutron-rich environments, a series of nuclear-mass models has been developed based on the Hartree–Fock–Bogoliubov (HFB) method with Skyrme and contact-pairing forces, together with phenomenological Wigner terms and correction terms for the spurious collective energy within the cranking approximation, the last one being HFB-32 [83]. In those HFB mass models, all the model parameters are fitted to essentially all the experimental mass data. While the first HFB-1 mass model aimed at proving that is was possible to reach a low root-mean-square (rms) deviation with respect to all experimental masses available at that time, most of the subsequent models were developed to systematically explore the parameter space or to take into account additional constraints. These include in particular a sensitivity study of the mass model accuracy and extrapolation to major changes in the description of the pairing interaction, the spin-orbit coupling or the nuclear matter properties, such as the effective mass, the symmetry energy and the stability of the equation of state.

With respect to the 2457 measured masses for $Z, N \geq 8$ nuclei [3], the 32 HFB mass models give an rms deviation ranging between 0.52 MeV for HFB-27 and 0.82 MeV for HFB-1. Recently, a new family of Skyrme-HFB models (BSkG) has been constructed using a three-dimensional coordinate-space representation, allowing for both axial and triaxial deformations during the adjustment process [84,85]. In particular, while nuclei with an odd number of nucleons were traditionally described within the so-called equal filling approximation, the BSkG2 mass model treats them on the same footing as even-even nuclei by breaking time-reversal symmetry, yielding an rms deviation of 0.68 MeV with respect to the 2457 known masses. These rms deviations can be compared to those obtained with other global mass models, such as the Gogny-HFB mass model with the D1M interaction [86] characterised by an rms of 0.81 MeV or the 2012 version of the finite-range droplet model (FRDM12) [87] with 0.61 MeV. However, when dealing with nuclei far away from stability, deviations between the HFB mass predictions can become significant, not only in the rigidity of the mass parabola, but also in the description of the shell gaps or pairing correlations [88]. The 1σ variance between the 32 HFB mass tables (with respect to the HFB-24 mass model) amounts to about 3 MeV, the largest deviations being found at the neutron drip line for the heaviest species. Such uncertainties can be interpreted as the model uncertainties (due to model defects) inherent to the given HFB model [89]. These model uncertainties have been shown to be significantly larger than the statistical uncertainties, i.e. those associated with local variations of the model parameters in the vicinity of an HFB minimum [88], as estimated using a variant of the Backward–Forward Monte Carlo method [90] to propagate the uncertainties on the masses of exotic nuclei far away from the experimentally known regions (note that this method considers only parameter sets that give rise to masses in reasonable agreement with experiments for all known nuclei).

Many effective interactions have been proposed to estimate nuclear structure properties within the relativistic or non-relativistic mean-field approaches [91]. Except the BSk and BSkG forces at the origin of the above-mentioned HFB mass models and the D1M interaction at the origin of the Gogny-HFB mass model [86], none of the other Skyrme or Gogny interactions have been fitted to the complete set of experimental masses. Consequently, their predictions lead to rms deviations typically larger than 2–3 MeV with respect to the bulk of known masses; e.g. masses obtained with the popular SLy4 force give an rms deviation of the order of 5 MeV [92]. Even the UNEDF0 and UNEDF1 interactions [93,94] fitted to about 72 nuclear masses end up with an rms deviation of 1.36 and 2.07 MeV on the full set of known data. With such a low accuracy, these mass models should not be used for r-process applications. Other global mass models have been developed, essentially within the macroscopic-microscopic approach, but this approach remains unstable with respect to parameter variations, as shown in the framework of the droplet model [95] and as illustrated in Fig. 4 between the FRDM12 [87] and WS4 [96] mass models, especially when approaching the neutron drip line. In addition, this approach suffers from major shortcomings, such as the incoherent link between the macroscopic part and the microscopic correction or the instability of the shell correction [81,82]. For this reason, more fundamental approaches, such as the mean field, are needed for astrophysical applications. The impact of mass models on the reaction rates along the Yb isotopic chain is illustrated in Fig. 3 (upper left panel) where deviations reaching 5 orders of magnitude can be observed for the most exotic neutron-rich Yb isotopes using HFB-31 [83] instead of the WS4 [96] masses.

When considering mass models obtained in relatively different frameworks, e.g the Skyrme-HFB or Gogny-HFB, large deviations are found in the mass predictions away from the experimentally known region. For example, as shown in Fig. 4, deviations up to typically ± 5 MeV can be observed for exotic nuclei between HFB-31 [83] and D1M [86] or BSkG2 [85] mass predictions, especially around the $N = 126$ and 184 shell closures. Neutron capture rates can consequently deviate by a few orders of magnitude with such mass differences, essentially due to different local variations in the pairing and shell description. Such deviations by far exceed what is acceptable for nucleosynthesis applications. For this reason, further improvements of mass models are required. These include development of relativistic as well as non-relativistic mean field models, but also the inclusion within such approaches of the state-of-the-art beyond-mean-field corrections, like the quadrupole or octupole correlations by the Generator Coordinate Method [97,98] and a proper treatment of odd-A and odd-odd nuclei with time-reversal symmetry breaking [85]. Such models should reproduce also as many experimental observables as possible. These include charge radii and neutron skin thicknesses, fission barriers and shape isomers, spectroscopic data such as the 2^+ energies, moments of inertia, but also infinite (neutron and symmetric) nuclear matter properties obtained from realistic calculations as well as specific observed or empirical properties of NS, like their maximum mass or mass-radius relations [99,100].

Future improvements should also take full advantage of the progress made in ab-initio methods in medium mass nuclei [101], such as many-body perturbation theory [102], self-consistent Green's function [103,104], coupled cluster [105], and in-medium similarity renormalization group [106]. These methods that used to be constrained to the description of nuclear properties for the $A \lesssim 100$ region, have now been extended successfully up to the $Z = 50$ region [107], starting solely from the knowledge of the fundamental two- and three-nucleon forces. If these ab-initio calcu-

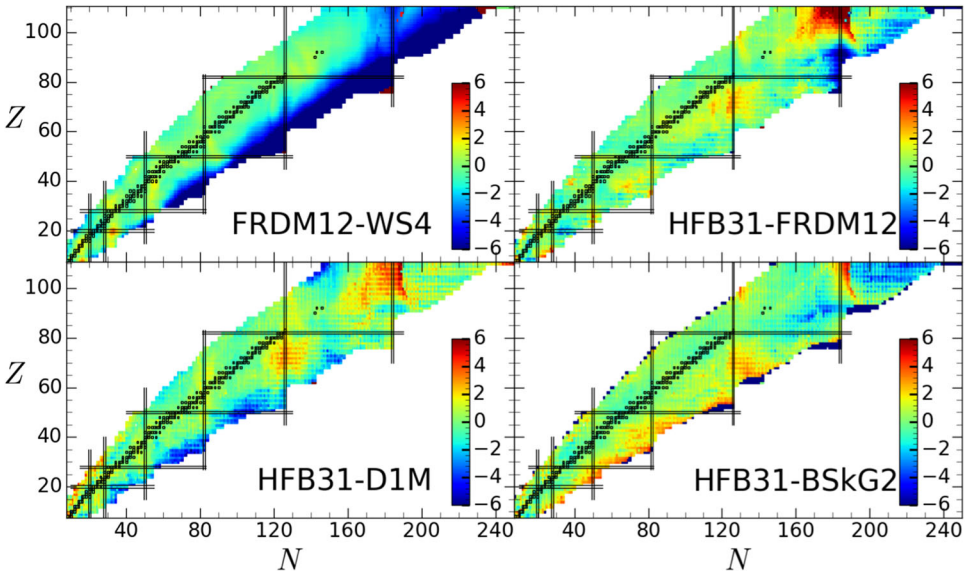

Fig. 4 Representation in the (N, Z) plane of the mass differences (in MeV) between the macroscpic-microscopic FRDM12 [87], WS4 [96] formulae and the mean-field HFB-31 [83], D1M [86], and BSkG2 [85] models for all the 8500 nuclei from $Z = 8$ up to $Z = 110$ between the BSkG2 proton and neutron driplines. The open squares correspond to the valley of β-stability. The double solid lines depict the neutron and proton magic numbers

lations have not reached yet the level of accuracy required in astrophysical applications, they may provide crucial guidance with the calculation of a few extremely exotic cases that could in the future constrain mean-field models.

4.2 Nuclear level densities

NLD play an essential role in reaction theory. Experimental information on NLD are usually restricted to low-lying levels, s- and p-wave resonance spacings [70,108], inelastic proton scattering [109] or model-dependent data extracted from the Oslo method [110]. Until recently, only classical analytical models of NLD were used for practical applications. In particular, the back-shifted Fermi gas model (BSFG) – or some variant of it – remains the most popular approach to estimate the spin-dependent NLD, particularly in view of its ability to provide a simple analytical formula [70,111]. However, none of the important shell, pairing and deformation effects are properly accounted for in any analytical description and therefore large uncertainties are expected, especially when extrapolating to very low (a few MeV) or high energies ($U \gtrsim 15$MeV) and/or to nuclei far from the valley of β-stability. Several approximations used to obtain the NLD expressions in an analytical form can be avoided by quantitatively taking into account the discrete structure of the single-particle spectra associated with realistic average potentials. This approach has the advantage of treating in a natural way shell, pairing and deformation effects on all the thermodynamic quantities [112]. Large scale calculations of NLD for nearly 8500 nuclei were also performed in the framework of the combinatorial method [113,114] and has proven its predictive power. One of the main advantages of the combinatorial approach is to provide not only the NLDs tabulated as a function of the excitation energy, but also the spin and parity distributions without any statistical assumption. In particular, it provides naturally non-Gaussian spin distributions as well as non-equipartition of parities which are known to have a significant impact on cross section predictions at low energies. Recent developments can now coherently take into account, for deformed nuclei, the transition to sphericity on the basis of a temperature-dependent Hartree-Fock calculation which provides at each temperature the structure properties needed to build the level densities [114]. These combinatorial models have proven their capacity to reproduce experimental data in a satisfactory way, in particular the s- and p-wave resonance spacings, cumulative number of low-lying level, and low-energy total NLD.

The impact of the NLD model on radiative neutron capture rates is illustrated in Fig. 3 (upper right panel) where the calculations have been performed either with the HFB plus combinatorial model [113] or the constant temperature (CT) plus Fermi Gas model [111]. Deviations up to a factor of 10 are found with a strong odd-even pattern. This shows how sensitive the neutron capture rates can be with respect to the NLD predictions. Still several improvements remain to be addressed, in particular at the lowest energies below the neutron separation energy, such as correlation effects, the treatment of the coupling between particle-hole and vibrational excited states, or the effect of triaxiality.

4.3 Optical potential

Though the phenomenological nucleon-nucleus optical potential of Woods–Saxon type [115] is still commonly used for astrophysical application, it is often replaced by the more microscopic potential derived from a Reid's hard core nucleon-nucleon interaction by applying the Brückner–Hartree–Fock approximation [116]. This so-called JLM poten-

tial has been updated by Bauge et al. [117] (hence JLMB) who empirically renormalized the energy dependence of the potential depth to reproduce scattering and reaction observables for spherical and quasi-spherical nuclei between ^{40}Ca and ^{209}Bi in a large energy range from the keV region up to 200 MeV. In this JLMB approach, the renormalization factors are rather well constrained by experimental data, except the low-energy regime of the λ_{W_1} factor affecting the isovector imaginary component. The major constraint imposed on the isovector component comes from the quasi-elastic (p, n) scattering data as well as the angle-integrated quasi-elastic (p, n) cross sections to the isobaric analog states at energies above some 20 MeV. For lower energies, the λ_{W_1} factor was extrapolated from the confident region around 20 MeV to a constant value of approximately 1.5. Due to the lack of scattering data in the keV region, the low-energy extrapolation of the λ_{W_1} factor remained essentially unconstrained.

It was shown that the isovector contribution to the imaginary component can be adjusted on experimental s-wave neutron strength function data ranging between 1 and 100 keV [118]. To describe the isospin dependence, a 30% increase of λ_{W_1} at energies below 1 MeV with respect to the JLMB value was considered in Ref. [118]. This modified potential (JLMB*) has been shown to improve the isospin dependence of the known s-wave neutron strength function of the long Sn and Te isotopic chains [118]. As observed in Fig. 3 (lower left panel), for the Yb isotopic chain, the potentials have in general a negligible impact on the radiative neutron capture cross section since within the statistical approach the (n, γ) channel is essentially dependent on the photon transmission coefficient. However, the experimental constraints introduced with JLMB* may have a drastic impact on the neutron capture rate. At large neutron excesses, the enhanced λ_{W_1} factor strongly reduces the imaginary component, i.e. the neutron absorption channel, and consequently the radiative neutron capture cross section. In particular, it can be seen that, for Yb isotopes with $N \gtrsim 135$, the rates obtained in JLMB* rapidly drop, leading to a totally insignificant resonant neutron capture. Before drawing any firm conclusion on the neutron capture by very neutron-rich nuclei, such a renormalisation of the isovector component of the imaginary potential in the keV region needs to be further constrained by additional theoretical and experimental works.

4.4 γ-ray strength function

The total photon strength function is one of the key ingredients for statistical cross section evaluation. Many experimental techniques, such as nuclear resonance fluorescence, the Oslo method, neutron resonance captures, the ratio method, inelastic proton scattering or photoreaction measurements, have been used to obtain information on the photon strength function and are reviewed in Refs. [71,119]. It is most frequently described in the framework of the phenomenological Lorentzian-type model of the giant dipole resonance (GDR) for both the $E1$ and $M1$ components [70,120,121]. Until recently, this model has even been the only one used for practical applications, and more specifically when global predictions are requested for large sets of nuclei.

The Lorentzian approach suffers, however, from shortcomings of various sorts. On the one hand, it is unable to predict the observed enhancement of the $E1$ strength below the neutron separation energy (for a review, see Ref. [71]). On the other hand, even if a Lorentzian function provides a suitable representation of the $E1$ strength, the location of its maximum and its width must be predicted from some underlying model for each nucleus. For astrophysics applications, these properties have often been obtained from a droplet-type model [122]. This approach clearly lacks reliability when dealing with exotic nuclei, as already demonstrated in Refs. [22,123].

In view of this situation, combined with the fact that the GDR properties and low-energy resonances may influence substantially the predictions of radiative capture cross sections, it is clearly of substantial interest to develop models of the microscopic type which will logically provide more reasonable reliability and predictive power for the dipole strength function. Attempts in this direction have been conducted within the QRPA model based on realistic Skyrme or Gogny interactions. Initially, the Skyrme BSk7 + QRPA model [123] introduced some phenomenological corrections to take the damping of the collective motion as well as the deformation effects into account. More recently, the Gogny D1M + QRPA model [124] allows for a consistent description of axially-symmetric deformations and includes phenomenologically beyond-mean-field corrections. Both models have proven their capacity to reproduce experimental photoabsorption data relatively well [71]. QRPA approaches lead to significant departures from a Lorentzian form, especially for neutron-rich nuclei.

HFB + QRPA calculations of the photoabsorption strength have been extended to the determination of the de-excitation strength function. Shell-model calculations of the de-excitation dipole strength function [125–127] as well as experimental data [128,129] suggest that at photon energies approaching the zero limit, the $E1$ strength remains constant while the $M1$ strength increases exponentially. It has been shown that, in a first approximation, the HFB + QRPA strength can be complemented by simple analytical expressions to account for the missing strength at the lowest energies approaching zero [71]. These contributions have been shown to reproduce satisfactorily experimental data at low energies, but also to affect significantly the calculation of the average radiative width as well as radiative nucleon capture cross sections. Although the additional dipole strength is located at low energies, typically below 3–

4 MeV, it impacts the overall radiative width, especially due to the increasing $M1$ strength at decreasing photon energies. As shown in Fig. 3, when approaching the neutron dripline, the radiative neutron capture rate calculated with D1M + QRPA strength [124] is seen to be a factor of about 100 larger than the one obtained with the Generalized Lorentzian (GLO) model [130]. The most significant effects responsible for such an increase are the low-energy $E1$ strength predicted for neutron-rich nuclei by the D1M + QRPA approach and the low-energy enhancement of the $M1$ de-excitation strength (the so-called $M1$ upbend).

However, QRPA calculations are known to fail reproducing the width (and even the position) of the GDR. To improve the prediction of the γ-ray strength function, especially at the low energies below the neutron threshold of relevance in radiative neutron captures, it is necessary to go beyond the QRPA scheme by including complex configurations as well as the coupling of single-particle with the phonon degrees of freedom (the so-called phonon coupling) [131–136]. The low-energy enhancement in the γ-ray strength function at very low energies (below 1–2 MeV) will need to be further investigated, experimentally as well as theoretically.

4.5 Fission

Since its discovery, fission has always been an active field of research both regarding its purely theoretical challenge and its practical applications [70,137,138]. Almost all existing evaluations of the neutron-induced fission cross sections rely on the multiple-humped fission penetration model where barriers are described by inverted decoupled parabolas. Such approaches consider all ingredients as free parameters to fit experimental cross sections [70,139]. Although such adjustments respond to the needs of some nuclear applications, their predictive power remains poor due to the large number of free parameters. Such methods should not be used in applications requiring a purely theoretical description of fission for experimentally unknown nuclei, such as nuclear astrophysics. Recent studies aim at providing more reliable descriptions of some of the basic nuclear ingredients required to describe fission cross sections. These concern in particular fission barriers (or more generally fission paths) and NLD at the fission saddle points, but also fission fragment distribution (FFD), including the average number of emitted neutrons. Recently, such nuclear ingredients have been systematically determined in the framework of mean field models for nuclear astrophysics applications, as described below.

4.5.1 Fission path

Detailed fission paths have been determined on the basis of the mean-field model [85,140,141] which has proven its capacity to estimate the static fission barrier heights with a relatively high degree of accuracy. The barriers determined within the HFB-14 [140] and BSkG2 models [85] reproduce the 45 empirical primary barriers [70] (i.e. the highest barriers of prime interest in cross section calculations) of nuclei with $Z \geq 90$ with an rms deviation as low as 0.61 MeV and 0.44 MeV, respectively. A similar accuracy is obtained (0.70 MeV and 0.47 MeV, respectively) for the secondary barriers. No theoretical models can claim to provide predictions of barrier heights with a global accuracy better than 0.5–1 MeV (in the best case), so that there is still a lot of room for improvement of global models in the prediction of fission barriers.

The determination of the fission path is also sensitive to number of degrees of freedom considered in the description of deformation. Global calculations of fission barriers for r-process nuclei assume axial symmetry but allow to break reflection symmetry since the outer barrier is known to be left-right asymmetric. Barriers are in many cases also triaxial and only a few calculations take such symmetry breaking into account [85,142,143]. Some recent relativistic mean-field studies even show that both non-axial and reflection asymmetric shapes need to be considered simultaneously for the description of potential energy surfaces and more particularly the outer fission barriers [85,143]. Such calculations still need to be applied more systematically to the exotic nuclei involved in the r-process.

4.5.2 Fission fragment distribution

The FFD as well as the number of emitted neutrons play a key role in nucleosynthesis simulations since they define which nuclei are produced by the fission recycling [72,144]. Both the Z- and A-dependencies of the fragment distribution need to be determined for all potentially fissioning nuclei. Since the widely-used Gaussian model of Kodoma and Takahashi [145], a number of new global scission-point models have been proposed and extended to exotic nuclei for astrophysical applications. These include in particular the so-called SPY model, corresponding to a renewed statistical scission-point model based on microscopic ingredients [146–148] and the so-called GEF model estimating the properties of the fission fragments and the emitted neutrons and photons in a global and semi-empirical way [149].

Both the SPY and GEF models predict significantly different FFDs, as illustrated in Fig. 5 where the yields of eight $A = 278$ isobars are shown. In the GEF case, the fragment distributions are mostly symmetrical for these particular fissioning nuclei (except for $Z = 97 - 99$), whereas a 4-peak distribution is predicted by SPY for all the corresponding isobars. Such doubly asymmetric fragment distributions have never been observed experimentally and can be traced back to the predicted Gogny-HFB potential energies at large deformations for the neutron-rich fragments favored

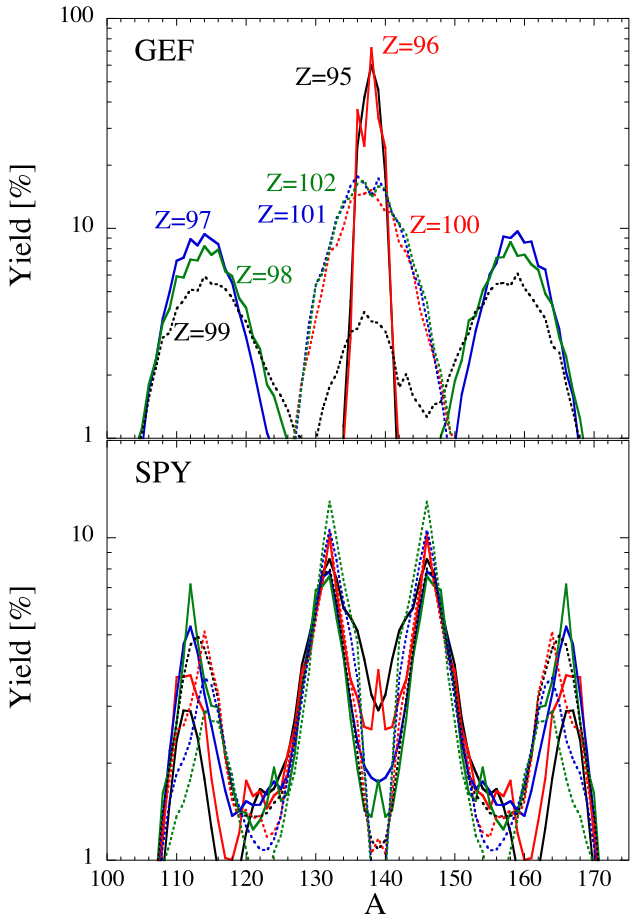

Fig. 5 FFDs predicted by the GEF (upper panel) and SPY models (lower panel) for 8 $A = 278$ isobars

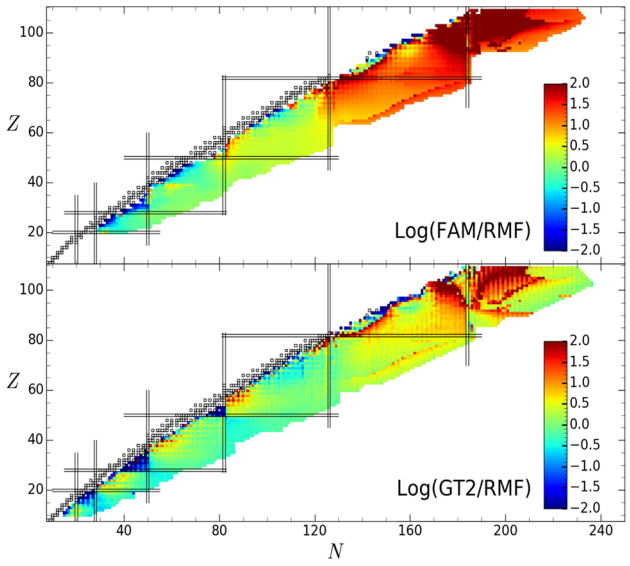

Fig. 6 Representation in the (N, Z) plane of the β-decay half-life ratios obtained by three global models. *Upper panel*: Ratio between the HFB plus FAM [156] and RMF + QRPA [155] predictions. *Lower panel*: Ratio between the HFB-21 + GT2 [152] and the RMF + QRPA [155] predictions. The open squares correspond to the stable nuclei or long-lived Th and U isotopes. The double solid lines depict the neutron and proton magic numbers

by the $A \simeq 278$ fission [144]. Detailed Gogny-HFB calculations of the potential energy surface in the parent fissioning nucleus have found qualitatively the presence of these two asymmetric fission modes [144], but such atypical fission modes still need to be confirmed experimentally.

5 β-decay rates

β-decay rates play a fundamental role in nuclear astrophysics in general [1,150]. Here, we will only focus on the application to the r-process nucleosynthesis [22,23] since they set the timescale of the nuclear flow and consequently of the production of the heavy elements. Most of the nuclei involved during the r-process neutron irradiation have yet to be discovered although β^- decay half-lives are known for about 1200 nuclei [151] among the 5000 required for r-process simulations. The use of theoretical models is therefore unavoidable [22]. For a proper prediction of the r-abundances in any r-process site, the β-decay rates need to be estimated within a factor smaller than typically 1.5.

Only a restricted number of global models of β-decay rates remains available for nucleosynthesis applications. These concern the macroscopic Gross Theory (GT2) [152], the FRDM+RPA [153], the Tamm–Dancoff approximation (TDA) [154], the relativistic mean-field (RMF) plus QRPA [155] or the HFB plus finite-amplitude method (FAM) [156]. The deviations between the predictions of the three GT2, RMF, FAM models are shown in Fig. 6 where ratios larger than a factor of 100 are found in many neutron-rich regions of the (N,Z) plane. In particular, for very heavy $Z \gtrsim 82$ nuclei, as well as along the isotonic chains corresponding to closed neutron shells ($N = 50, 82, 126, 184$), responsible for the formation of the r-process peaks observed in the solar system, non-negligible differences can be observed, leading to different estimated r-process peak structures [72].

Here also, more effort is needed to include not only the contribution of the forbidden transitions [155,156] but also the deformation effects, the majority of nuclei being deformed [157]. Recent studies within the fully self-consistent proton-neutron QRPA model using the finite-range Gogny interaction have now also taken axially symmetric deformations consistently into account [157], but forbidden transitions remain to be included. The inclusion of finite-temperature effects as well as the phonon coupling has also been shown to give rise to a redistribution of the Gamow-Teller strength and impact the β-decay half-lives of neutron-rich nuclei significantly [158]. Further progress along all these lines will hopefully help to improve the predictions.

Finally, note that on the basis of the β-decay strength, the β-delayed processes, including neutron emission and fission for the heaviest species, need to be derived. Detailed calculations on the basis of statistical reaction codes, like TALYS [79], can take full account of the competition of the various open channels (neutron, photon, fission) in the daughter nucleus. Reaction models still need to be better exploited to estimate the probability for such β-delayed processes.

6 Conclusion

A prodigious amount of nuclear data for thousands of nuclei is needed for nuclear astrophysics applications. This challenges experimental techniques, but especially the robustness and predictive power of the necessary nuclear models. For the last decades, important progress has been achieved both through new measurements and through the development of improved nuclear models. Despite such effort, experimental data only cover a minute fraction of the whole set of data required. To fill the gaps, only theoretical predictions can be used. It is now feasible to use more reliable, but also more complex microscopic or semi-microscopic models in the evaluation and prediction of nuclear data for astrophysical applications. A microscopic description by a physically sound model based on first principles ensures a reliable extrapolation away from experimentally known region, but a necessary condition for application remains: such models should be able to compete with the often more locally accurate, but more phenomenological highly parametrized models in reproducing experimental data. The accuracy and reliability of our predictions today are still far from being at the level of the requirements of nuclear astrophysics applications. A continued effort to improve our predictions of the reaction and β-decay rates, including their statistical and systematic uncertainties, for nuclei far away from stability is obviously required. Priority should be given to a better description of the ground-state, fission and β-decay properties, but also NLD, optical potential and γ-ray strength functions. A huge amount of work is still needed to take full advantage of the development of state-of-the-art microscopic models in building universal models that include as much as possible the microscopic character of quantum physics. This effort to improve microscopic nuclear predictions is concomitant with new development aiming at improving the description of the reaction mechanisms, including the equilibrium, pre-equilibrium and direct capture processes. This theoretical work requires in parallel new measurements of structure properties far away from stability, but also reaction cross sections on stable targets and any experiments that can provide new insight on the numerous ingredients of the reaction models and their extrapolation far away from the valley of β-stability.

Acknowledgements S.G. is F.R.S.-FNRS research associate.

Data availability statement This manuscript has no associated data or the data will not be deposited. [Authors' comment: There is no associated data to the paper.]

References

1. M. Arnould, S. Goriely, Prog. Part. Nucl. Phys. **112**, 103766 (2020)
2. C. Iliadis, *Nuclear Physics of Stars*, 2nd edn. (Wiley-VCH, New York, 2015)
3. M. Wang, W. Huang, F. Kondev, G. Audi, S. Naimi, Chin. Phys. C **45**, 030003 (2021)
4. V. Tatischeff, S. Gabici, Ann. Rev. Nucl. Part. Sci. **68**, 377 (2018)
5. C. Pitrou, A. Coc, J.P. Uzan, E. Vangioni, Phys. Rep. **754**, 1 (2018)
6. B. Metzger, G. Martínez-Pinedo, S. Darbha, E. Quataert, A. Arcones, D. Kasen, R. Thomas, P. Nugent, I.V. Panov, N.T. Zinner, MNRAS **406**, 2650 (2010)
7. A. Bauswein, S. Goriely, H.T. Janka, Astrophys. J. **773**, 78 (2013)
8. S. Woosley, T. Weaver, Astrophys. J. Suppl. S. **101**, 181 (1995)
9. M. Limongi, A. Chieffi, Astrophys. J. Suppl. S **237**, 13 (2018)
10. F. Käppeler, H. Beer, K. Wisshak, Rep. Prog. Phys. **52**, 945 (1989)
11. S. Goriely, N. Mowlavi, A&A **362**, 599 (2000)
12. A.I. Karakas, J.C. Lattanzio, Pub. Astron. Soc. Pac. **31**, e030 (2014). arXiv:1405.0062
13. S. Goriely, L. Siess, Astron. Astrophys. **609**, A29 (2018)
14. A. Choplin, R. Hirschi, G. Meynet, S. Ekström, C. Chiappini, A. Laird, Astron. Astrophys. **618**, A133 (2018)
15. J. Cowan, W. Rose, Astrophys. J. **212**, 149 (1977)
16. F. Herwig, M. Pignatari, P.R. Woodward, D.H. Porter, G. Rockefeller, C.L. Fryer, M. Bennett, R. Hirschi, Astophys. J **727**, 89 (2011). arXiv:1002.2241
17. M. Hampel, R.J. Stancliffe, M. Lugaro, B.S. Meyer, Astrophys. J. **831**, 171 (2016). arXiv:1608.08634
18. O. Clarkson, F. Herwig, M. Pignatari, Mon. Not. R. Astron. Soc. **474**, L37 (2018)
19. P.A. Denissenkov, F. Herwig, P. Woodward, R. Andrassy, M. Pignatari, S. Jones, Mon. Not. R. Astron. Soc. **488**, 4258 (2019). arXiv:1809.03666
20. A. Choplin, L. Siess, S. Goriely, A&A **648**, A119 (2021)
21. S. Goriely, L. Siess, A. Choplin, A&A **654**, A129 (2021)
22. M. Arnould, S. Goriely, K. Takahashi, Phys. Rep. **450**, 97 (2007)
23. J. Cowan, C. Sneden, J. Lawler, A. Aprahamian, M. Wiescher, K. Langanke, G. Martínez-Pinedo, F.K. Thielemann, Rev. Mod. Phys. **93**, 015002 (2021)
24. M. Rayet, M. Arnould, M. Hashimoto et al., Astron. Astrophys. **298**, 517 (1995)
25. M. Arnould, S. Goriely, Phys. Rep. **384**, 1 (2003)
26. C. Travaglio, T. Rauscher, A. Heger, M. Pignatari, C. West, Astrophys. J. **854**, 18 (2018)
27. Y. Génolini, D. Maurin, I.V. Moskalenko, M. Unger, Phys. Rev. C **98**, 034611 (2018)
28. W.D. Arnett, *Supernovae and Nucleosynthesis* (Princeton University Press, Princeton, 1996)
29. M. Limongi, O. Staniero, A. Chieffi, Astrophys. J. Suppl. S **129**, 625 (2000)
30. U. Battino, M. Pignatari, C. Ritter, F. Herwig, P. Denisenkov, J.W. Den Hartogh, R. Trappitsch, R. Hirschi, B. Freytag, F. Thielemann et al., Astrophys. J **827**, 30 (2016). arXiv:1605.06159
31. G. Meynet, S. Ekström, A. Maeder, Astron. Astrophys. **447**, 623 (2006)
32. U. Frischknecht, R. Hirschi, M. Pignatari et al., Mon. Not. R. Astron. Soc. **456**, 1803 (2016)

33. S. Goriely, M. Arnould, Astron. Astrophys. **312**, 327 (1996)
34. R. Hoffman, S. Woosley, Y.Z. Qian, Astrophys. J. **482**, 951 (1997)
35. H.T. Janka, *Handbook of Supernovae* (Springer International Pub. AG, Cham, 2017)
36. S. Wanajo, B. Müller, H.T. Janka, A. Heger, Astrophys. J. **853**, 40 (2018)
37. H.T. Janka, Ann. Rev. Nucl. Part. Sci. **62**, 407 (2012)
38. D. Siegel, J. Barnes, B. Metzger, Nature **569**, 241 (2019)
39. O. Just, S. Goriely, H.T. Janka, S. Nagataki, A. Bauswein, MNRAS **509**, 1377 (2022)
40. O. Just, M.A. Aloy, M. Obergaulinger, S. Nagataki, Astrophys. J. Lett. **934**, L30 (2022)
41. P. Mösta, L. Roberts, G. Halevi, C. Ott, J. Lippuner, R. Haas, E. Schnetter, Astophys. J. **864**, 171 (2018)
42. M. Reichert, M. Obergaulinger, M. Eichler, M.Á. Aloy, A. Arcones, MNRAS **501**, 5733 (2021)
43. C. Winteler, R. Käppeli, A. Perego, A. Arcones, N. Vasset, N. Nishimura, M. Liebendörfer, F.K. Thielemann, Astrophys. J. **750**, L22 (2012)
44. L. Roberts, D. Kasen, W. Lee, E. Ramirez-Ruiz, Astrophys. J. Lett. **736**, L21 (2011)
45. S. Goriely, A. Bauswein, H.T. Janka, Astrophys. J. Lett. **738**, L32 (2011)
46. O. Just, A. Bauswein, R. Ardevol Pulpillo, S. Goriely, H.T. Janka, MNRAS **448**, 541 (2015)
47. A. Bauswein, R. Ardevol Pulpillo, H.T. Janka, S. Goriely, Astrophysical J. Lett **773**, L9 (2014)
48. S. Wanajo, Y. Sekiguchi, N. Nishimura, K. Kiuchi, K. Kyutoku, M. Shibata, Astrophys. J. Lett. **789**, L39 (2014)
49. Y. Sekiguchi, K. Kiuchi, K. Kyutoku, M. Shibata, Phys. Rev. D **91**, 064059 (2015)
50. D. Radice, A. Perego, K. Hotokezaka, S.A. Fromm, S. Bernuzzi, L.F. Roberts, Astrophys. J **869**, 130 (2018). arXiv:1809.11161
51. V. Nedora, S. Bernuzzi, D. Radice, B. Daszuta, A. Endrizzi, A. Perego, A. Prakash, M. Safarzadeh, F. Schianchi, D. Logoteta, Astrophys. J. **906**, 98 (2021)
52. B. Abbott, R. Abbott, T. Abbott et al., Phys. Rev. Lett. **119**, 161101 (2017)
53. D. Watson, C.J. Hansen, J. Selsing, A. Koch, D.B. Malesani, J.P.U.F. Anja, C. Andersen, A. Arcones, A. Bauswein, S. Covino, A. Grado et al., Nature **574**, 497 (2019)
54. J.H. Gillanders, S.J. Smartt, S.A. Sim, A. Bauswein, S. Goriely, Mon. Not. R. Astron. Soc. **515**, 631 (2022)
55. A. Choplin, S. Goriely, R. Hirschi, N. Tominaga, G. Meynet, Astron. Astrophys. **661**, A86 (2022)
56. K. Nomoto, F.K. Thielemann, K. Yokoi, Astrophys. J. **286**, 644 (1984)
57. C. Travaglio, R. Gallino, T. Rauscher, F. Röpke, W. Hillebrandt, Astrophys. J. **799**, 54 (2015)
58. S. Goriely, D. Garcia-Senz, E. Bravo, J. José, Astron. Astrophys. **444**, L1 (2005)
59. C. Fröhlich, G. Martínez-Pinedo, M. Liebendörfer, F.K. Thielemann, E. Bravo, W.R. Hix, K. Langanke, N.T. Zinner, Phys. Rev. Lett. **96**, 142502 (2006)
60. C. Angulo, M. Arnould, M. Rayet et al., Nucl. Phys. A **656**, 3 (1999)
61. Y. Xu, S. Goriely, A. Jorissen, G. Chen, M. Arnould, A&A **549**(10), A106 (2013)
62. A.L. Sallaska, C. Iliadis, A.E. Champagne, S. Goriely, S. Starrfield, F. Timmes, ApJS **207**, 18 (2013)
63. D. Yakovlev, L. Gasques, A. Afanasjev, M. Beard, M. Wiescher, Phys. Rev. C **74**, 035803 (2006)
64. A. Potekhin, G. Chabrier, Contrib. Plasma Phys. **53**, 397 (2013)
65. N. Colonna, F. Gunsing, F. Käppeler, Prog. Part. Nucl. Phys. **101**, 177 (2018)
66. F. Käppeler, F.K. Thielemann, M. Wiescher, Annu. Rev. Nucl. Part. Sci. **48**, 175 (1998)
67. I. Dillmann, T. Szücs, R. Plag, Z. Fülöp, F. Käppeler, A. Mengoni, T. Rauscher, Nucl. Data Sheets **120**, 171 (2014)
68. O. Roig, G. Bélier, V. Méot, D. Abt, J. Aupiais, J.M. Daugas, C. Jutier, G.L. Petit, A. Letourneau, F. Marie et al., Phys. Rev. C **74**, 054604 (2006)
69. O. Roig, V. Méot, B. Rossé, G. Bélier, J.M. Daugas, A. Letourneau, A. Menelle, P. Morel, Phys. Rev. C **83**, 064617 (2011)
70. R. Capote, M. Herman, P. Oblozinsky, P. Young, S. Goriely, T. Belgya, A. Ignatyuk, A. Koning, S. Hilaire, V. Plujko et al., Nucl. Data Sheets **110**, 3107 (2009)
71. S. Goriely, P. Dimitriou, M. Wiedeking, T. Belgya, R. Firestone, J. Kopecky, M. Krticka, V. Plujko, R. Schwengner, S. Siem et al., Eur. Phys. J. A **55**, 172 (2019)
72. S. Goriely, Eur. Phys. J. A **51**, 22 (2015)
73. J. Lynn, *The Theory of Neutron Resonance Reactions* (Clarendon press, Oxford, 1968)
74. G. Satchler, *Introduction to Nuclear Reactions* (Macmillan Press Ltd., New York, 1980)
75. P. Descouvemont, J. Phys. G Nucl. Part. Phys. **35**, 014006 (2008)
76. Y. Xu, S. Goriely, Phys. Rev. C **86**, 045801 (2012)
77. Y. Xu, S. Goriely, A.J. Koning, S. Hilaire, Phys. Rev. C **90**, 024604 (2014)
78. D. Rochman, S. Goriely, A. Koning, H. Ferroukhi, Phys. Lett. B **764**, 109 (2017)
79. A.J. Koning, D. Rochman, Nucl. Data Sheets **113**, 2841 (2012)
80. S. Hilaire, S. Goriely, S. Péru, N. Dubray, M. Dupuis, E. Bauge, Eur. Phys. J. A **52**, 336 (2016)
81. D. Lunney, J. Pearson, C. Thibault, Rev. Mod. Phys. **75**, 1021 (2003)
82. J.M. Pearson, Hyp. Int. **132**, 59 (2001)
83. S. Goriely, N. Chamel, J.M. Pearson, Phys. Rev. C **93**, 034337 (2016)
84. G. Scamps, S. Goriely, E. Olsen, M. Bender, W. Ryssens, Eur. Phys. J. A **57**, 333 (2021)
85. W. Ryssens, G. Scamps, S. Goriely, M. Bender, Eur. Phys. J. A **58**, 246 (2022)
86. S. Goriely, S. Hilaire, M. Girod, S. Péru, Phys. Rev. Lett. **102**, 242501 (2009)
87. P. Möller, A. Sierk, T. Ichikawa, H. Sagawa, At. Data Nucl. Data Tables **109–110**, 1 (2016)
88. S. Goriely, R. Capote, Phys. Rev. C **89**, 054318 (2014)
89. D. Neudecker, R. Capote, H. Leeb, Nucl. Instrum. Methods Phys. Res. A **723**, 163 (2013)
90. E. Bauge, P. Dossantos-Uzarralde, J. Korean Phys. Soc. **59**, 1218 (2011)
91. M. Bender, P.H. Heenen, P.G. Reinhard, Rev. Mod. Phys. **75**, 121 (2003)
92. M. Stoitsov, J. Dobaczewski, W. Nazarewicz, S. Pittel, D. Dean, Phys. Rev. C **68**, 054312 (2003)
93. M. Kortelainen, T. Lesinski, J. Moré, W. Nazarewicz, J. Sarich, N. Schunck, M.V. Stoitsov, S.M. Wild, Phys. Rev. C **82**, 024313 (2010)
94. M. Kortelainen, J. McDonnell, W. Nazarewicz, P.G. Reinhard, J. Sarich, N. Schunck, M.V. Stoitsov, S.M. Wild, Phys. Rev. C **85**, 024304 (2012)
95. S. Goriely, M. Arnould, Astron. Astrophys. **262**, 73 (1992)
96. N. Wang, M. Liu, X. Wu, J. Meng, Phys. Lett. B **734**, 215 (2014)
97. M. Bender, G. Bertsch, P.H. Heenen, Phys. Rev. C **73**, 034322 (2006)
98. L. Robledo, T. Rodríguez, R. Rodríguez-Guzmán, J. Phys. G Nucl. Part. Phys. **46**, 013001 (2018)
99. A.F. Fantina, J.M.P.N. Chamel, S. Goriely, Astron. Astrophys. **559**, A128 (2013)

100. J.M. Pearson, N. Chamel, A.Y. Potekhin, A.F. Fantina, C. Ducoin, A.K. Dutta, S. Goriely, MNRAS **481**, 2994 (2018)
101. H. Hergert, Front. Phys. **8**, 379 (2020)
102. A. Tichai, R. Roth, T. Duguet, Front. Phys. **8**, 164 (2020)
103. V. Soma, Front. Phys. **8**, 340 (2020)
104. C. Barbieri, T. Duguet, V. Somà, Phys. Rev. C **105**, 044330 (2022)
105. G. Hagen, T. Papenbrock, M. Hjorth-Jensen, D.J. Dean, Rep. Prog. Phys. **77**, 096302 (2014)
106. H. Hergert, S. Bogner, T. Morris, A. Schwenk, K. Tsukiyama, Phys. Rep. **621**, 165 (2016)
107. T. Miyagi, S.R. Stroberg, P. Navrátil, K. Hebeler, J.D. Holt, Phys. Rev. C **105**, 014302 (2022)
108. S. Mughabghab, *Atlas of Neutron Resonances: Resonance Parameters and Thermal Cross Sections. Z= 1–100* (Elsevier, Amsterdam, 2006)
109. S. Bassauer, P. Von Neumann-Cosel, A. Tamii, Phys. Rev. C **94**, 054313 (2016)
110. A. Schiller, L. Bergholt, M. Guttormsen, E. Melby, J. Rekstad, S. Siem, Nucl. Instrum. Methods Phys. Res. A **447**, 498 (2000)
111. A.J. Koning, S. Hilaire, S. Goriely, Nucl. Phys. A **810**, 13 (2008)
112. P. Demetriou, S. Goriely, Nucl. Phys. A **695**, 95 (2001)
113. S. Goriely, S. Hilaire, A.J. Koning, Phys. Rev. C **78**, 064307 (2008)
114. S. Hilaire, M. Girod, S. Goriely, A.J. Koning, Phys. Rev. C **86**, 064317 (2012)
115. A.J. Koning, J. Delaroche, Nucl. Phys. A **713**, 231 (2003)
116. J. Jeukenne, A. Lejeune, C. Mahaux, Phys. Rev. C **16**, 80 (1977)
117. E. Bauge, J.P. Delaroche, M. Girod, Phys. Rev. C **63**, 024607 (2001)
118. S. Goriely, J.P. Delaroche, Phys. Lett. B **653**, 178 (2007)
119. A. Zilges, D. Balabanski, J. Isaak, N. Pietralla, Prog. Part. Nucl. Phys. **122**, 103903 (2022)
120. V. Plujko, O. Gorbachenko, R. Capote, P. Dimitriou, At. Data Nucl. Data Tables **123**, 1 (2018)
121. S. Goriely, V. Plujko, Phys. Rev. C **99**, 014303 (2019)
122. W. Myers, W. Swiatecki, T. Kodama, L.J. El-Jaick, E.R. Hilf, Phys. Rev. C **15**, 2032 (1977)
123. S. Goriely, E. Khan, M. Samyn, Nucl. Phys. A **739**, 331 (2004)
124. S. Goriely, S. Hilaire, S. Péru, K. Sieja, Phys. Rev. C **98**, 014327 (2018)
125. K. Sieja, Phys. Rev. Lett. **119**, 052502 (2017)
126. K. Sieja, EPJ Web Conf. **146**, 05004 (2017)
127. R. Schwengner, S. Frauendorf, B.A. Brown, Phys. Rev. Lett. **118**, 092502 (2017)
128. A. Voinov, E. Algin, U. Agvaanluvsan, T. Belgya, R. Chankova, M. Guttormsen, G.E. Mitchell, J. Rekstad, A. Schiller, S. Siem, Phys. Rev. Lett. **93**, 142504 (2004)
129. M. Guttormsen, R. Chankova, U. Agvaanluvsan, E. Algin, L.A. Bernstein, F. Ingebretsen, T. Lönnroth, S. Messelt, G.E. Mitchell, J. Rekstad et al., Phys. Rev. C **71**, 044307 (2005)
130. J. Kopecky, M. Uhl, Phys. Rev. C **41**, 1941 (1990)
131. N. Tsoneva, H. Lenske, Phys. Rev. C **77**, 024321 (2008)
132. P. Papakonstantinou, R. Roth, Phys. Lett. B **671**, 356 (2009)
133. O. Achakovskiy, A. Avdeenkov, S. Goriely, S. Kamerdzhiev, S. Krewald, Phys. Rev. C **91**, 034620 (2015)
134. D. Gambacurta, M. Grasso, O. Vasseur, Phys. Lett. B **777**, 163 (2018)
135. E. Litvinova, P. Ring, V. Tselyaev, Phys. Rev. C **88**, 044320 (2013)
136. I.A. Egorova, E. Litvinova, Phys. Rev. C **94**, 034322 (2016)
137. N. Schunck, L. Robledo, Rep. Prog. Phys. **79**, 116301 (2016)
138. N. Schunck, Prog. Part. Nucl. Phys. **125**, 103963 (2022)
139. S. Bjørnholm, J. Lynn, Rev. Mod. Phys. **52**, 725 (1980)
140. S. Goriely, M. Samyn, M.J. Pearson, Phys. Rev. C **75**, 064312 (2007)
141. J.F. Lemaître, S. Goriely, S. Hilaire, N. Dubray, Phys. Rev. C **98**, 024623 (2018)
142. J.P. Delaroche, M. Girod, H. Goutte, J. Libert, Nucl. Phys. A **771**, 103 (2006)
143. B.N. Lu, J. Zhao, E.G. Zhao, S.G. Zhou, Phys. Rev. C **89**, 014323 (2014)
144. S. Goriely, J.L. Sida, J.F. Lemaître, S. Panebianco, N. Dubray, S. Hilaire, A. Bauswein, H.T. Janka, Phys. Rev. Lett. **111**, 242502 (2013)
145. T. Kodoma, K. Takahashi, Nucl. Phys. A **239**, 489 (1975)
146. S. Panebianco, J.L. Sida, H. Goutte, J.F. Lemaitre, N. Dubray, S. Hilaire, Phys. Rev. C **86**, 064601 (2012)
147. J.F. Lemaître, S. Goriely, S. Hilaire, J.L. Sida, Phys. Rev. C **99**, 034612 (2019)
148. J.F. Lemaître, S. Goriely, A. Bauswein, H.T. Janka, Phys. Rev. C **103**, 025806 (2021)
149. K.H. Schmidt, B. Jurado, C. Amouroux, C. Schmitt, Nucl. Data Sheets **131**, 107 (2016)
150. T. Suzuki, Prog. Part. Nucl. Phys. **126**, 103974 (2022)
151. F. Kondev, M. Wang, W. Huang, S. Naimi, G. Audi, Chin. Phys. C **45**, 030001 (2021)
152. T. Tachibana, M. Yamada, Y. Yoshida, Prog. Theor. Phys. **84**, 641 (1990)
153. P. Möller, B. Pfeiffer, K.L. Kratz, Phys. Rev. C **67**, 055802 (2003)
154. H. Klapdor, J. Metzinger, T. Oda, At. Data Nucl. Data Tables **31**, 81 (1984)
155. T. Marketin, L. Huther, G. Martinez-Pinedo, Phys. Rev. C **93**, 025805 (2016)
156. E.M. Ney, J. Engel, T. Li, N. Schunck, Phys. Rev. C **102**, 034326 (2020)
157. M. Martini, S. Péru, S. Goriely, Phys. Rev. C **89**, 044306 (2014)
158. E. Litvinova, C. Robin, H. Wibowo, Phys. Lett. B **800**, 135134 (2020)

Springer Nature or its licensor (e.g. a society or other partner) holds exclusive rights to this article under a publishing agreement with the author(s) or other rightsholder(s); author self-archiving of the accepted manuscript version of this article is solely governed by the terms of such publishing agreement and applicable law.